Carbon nanotube-based mixed-matrix membranes with supramolecularly engineered interface for enhanced gas separation performance

Qinnan Zhang, Si Li, Ceming Wang, Hsueh-Chia Chang, Ruilan Guo *

Department of Chemical and Biomolecular Engineering, University of Notre Dame, Notre Dame, IN, 46556, United States

A B S T R A C T

In this study, novel nanocomposite membranes were fabricated from single-walled carbon nanotubes (SWNTs) and a triptycene-containing polyimide. The desirable interfacial morphology and homogenous dispersion of SWNTs were achieved by strong π-π stacking and supramolecular shape-fitting interactions between the nanotube and the paddlewheel-shaped triptycene moieties in polymer matrix. Mixed-matrix membranes (MMMs) containing 2–15 wt% of as-purchased SWNTs (AP-SWNTs) were prepared and tested for their gas transport properties. While all MMMs showed greatly enhanced permeabilities with well-maintained selectivities, a non-linear dependence of permeability on filler content was observed. Another series of MMMs with purified SWNTs (P-SWNTs) and acid-treated SWNT (A-SWNTs) were also prepared. The functionalized A-SWNT MMM exhibited the best separation performance at 2 wt% filler content among all MMMs, which can be attributed to the improved interfacial affinity with carboxylic acid functionalized surface of A-SWNTs.

1. Introduction

Membrane technology for gas separation grows steadily in the past few decades, as it provides the opportunity for developing separation processes with high energy efficiency, low operation cost and simple installation, and low carbon footprint [1–3]. However, the separation performance of polymeric membranes is generally limited by the trade-off relationship between permeability and selectivity, as manifested in Robeson's upper bound plots [4,5]. On the other hand, many researchers have strived to explore inorganic membrane materials, where some of them exhibited outstanding separation performance that surpasses the upper bound [6,7]. However, those type of materials generally suffer from high cost and difficulties in scale-up [8]. To circumvent the problems, a feasible approach is to fabricate membranes that combine inorganic fillers with a polymer matrix, yielding mixed-matrix membranes (MMMs). Ideally, the composite membranes should take advantages of both the filler (e.g., fast and selective gas transport) and polymer (e.g., processability, stability) phases [9,10].

Despite their great potential, the fabrication of MMMs is still facing the challenges of incompatibility between fillers and polymer matrix, leading to inhomogeneous filler dispersion and interfacial defects that deteriorate separation performance and mechanical integrity [11–14]. Therefore, it is critical to control and optimize the interfacial interactions for defect-free composite membranes enabling the synergetic effects of both filler and polymer phases via proper selection and "matching" of filler and polymer combinations that have intrinsically good gas transport properties, as well as strong affinity between the two phases [13,15,16].

Among the many studied fillers, carbon nanotubes (CNTs) have been studied intensively because of their excellent mechanical properties that are ideal for robust composite materials [17,18]. More importantly, gas transport inside the carbon nanotubes is extremely fast, which can be orders of magnitude higher than commonly used porous materials, such as zeolite [19,20]. The ultra-high transport rate is a result of the inherent ultrahigh smoothness of inner carbon walls [21,22]. It suggests the potential benefit of incorporating carbon nanotubes in MMMs for improving gas permeabilities. For example, Khan et al. found that the addition of 2 wt% pristine and functionalized single-walled carbon nanotubes (SWNTs) and multi-walled carbon nanotubes (MWNTs) into a polymer of intrinsic microporosity (PIM) enhanced the permeabilities of CO_2, N_2 and CH_4 [23]. Sun et al. reported the fabrication of MMMs based on acid-treated MWNTs and a polyimide using *in-situ* polymerization, which showed an increase in CO_2 permeability by 292% and an equally obvious increased CO_2/N_2 selectivity at 3 wt% filler loading [24]. Recently, amine and carboxylic acid modified MWNTs were incorporated in Pebax-1657 and studied by Habibiannejad et al. They revealed

that the gas separation performance remarkably relies on the surface functionality, the penetrant properties and the operating conditions. The 4 wt% NH_2 functionalized MWNT/Pebax composite membrane showed outstanding CO_2/N_2 separation performance that passed the upper bound limit [25]. While these studies demonstrated the benefits of improved permeability via incorporating CNTs, the carbon nanotubes based MMMs sometimes encountered the interfacial defects and agglomeration, especially at high loadings, due to the strong van der Waals forces between nanotubes and the large aspect ratio of long bundles of CNTs [20,26,27].

To address the interfacial incompatibility issue in most CNT-based mixed-matrix membranes, a new CNT-polyimide combination is studied in this work. Specifically, a polyimide containing hierarchical triptycene units (6FDA-TP) [28] is used as polymer matrix, in which triptycene units may introduce π-π stacking and supramolecular shape-fitting interactions with CNTs enabling the formation of ideal interface morphology in composite membranes (Fig. 1). Triptycene is composed of three fused benzene rings in a paddlewheel-like shape [29, 30]. The rigid, bulky structure can disrupt efficient polymer chain packing to introduce additional free volume for fast gas diffusion. More importantly, the unique spatial configuration allows it to interact with carbon nanotubes via nano-confinement effect and π-π stacking interaction which promotes CNTs dispersion as well as improve interfacial compatibility. For example, Li et al. reported a supramolecular complex of water-soluble triptycene derivatives and SWNTs, which could form a homogeneous aqueous solution stable for months [31]. In this work, a series of new MMMs were fabricated by incorporating SWNTs into 6FDA-TP polyimide. MMMs with 2–15 wt% of as-purchased SWNTs (AP-SWNTs) were fabricated to study the effect of filler loading on gas transport properties. Additionally, purified SWNTs (P-SWNTs) and acid-treated (A-SWNTs) were prepared, characterized and used to cast MMMs to examine the effects of nanotube length and surface functionality. The obtained membranes were comprehensively examined and characterized in terms of morphology (by SEM) and physical properties. Pure gas permeation tests were performed with five different gases to investigate the gas transport properties of the composite membranes, which are correlated with membrane morphology to elucidate structure-property relationship for this new series of CNT-based mixed-matrix membranes.

2. Experimental

2.1. Materials

Pristine single-walled carbon nanotubes (AP-SWNTs) were purchased from Carbon Solution Inc. Nitric acid (HNO_3, 67%–70%) and sulfuric acid (H_2SO_4, 96%) were obtained from BDH and EMD Milipore, respectively. 4,4′-hexafluoroisopropylidine bisphthalic dianhydride (6FDA, 99%) was purchased from Akron Polymer Systems and dried at 160 °C overnight prior to use. Anhydrous pyridine (99.8%) and anhydrous dimethylacetamide (DMAc, 99.8%) were purchased from EMD. 2-fluoro-5-nitrobenzotrifluoride (99%) was obtained from Matrix Scientific. All other chemicals were obtained from Sigma-Aldrich and used without further treatment.

2.2. Preparation of purified SWNTs (P-SWNTs) and shortened SWNTs (A-SWNTs)

AP-SWNTs were purified by refluxing in 3 M HNO_3 for 12 h. The solution was diluted in DI water and the black solid was collected by filtering through a 0.45 μm pore-sized PTFE membrane. The collected product was rinsed with DI water and dried at room temperature producing purified P-SWNTs.

The purified SWNTs (P-SWNTs) were cut into shorter length by a treatment using a HNO_3 and H_2SO_4 mixture (3:1) with sonication for 6 h at room temperature. Then, the mixture was filtered and washed with DI water till the pH of the filtrate indicated it was neutralized. The final product, i.e., A-SWNTs, was dried in vacuum oven at 80 °C overnight.

2.3. Synthesis of 6FDA-TP polyimide as polymer matrix

6FDA-TP polyimide (Fig. 2) was synthesized according to the procedure reported by our group previously (named "6FDA-1,4-trip_CF_3" in this report) [28]. In general, a triptycene-1,4-diamine with high purity was prepared. Then, the diamine was polymerized with commercial 6FDA to obtain polyimide using chemical imidization method. The obtained white fibrous polymer was dried and stored for the composite membrane preparation.

2.4. Preparation of mixed-matrix membranes from 6FDA-TP polyimide and various SWNT series
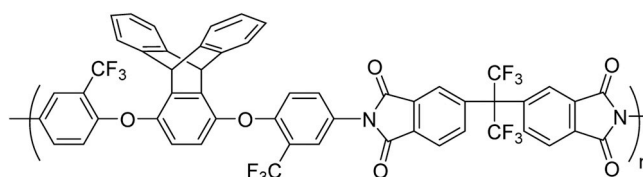
The general fabrication of the AP-SWNT/6FDA-TP composite

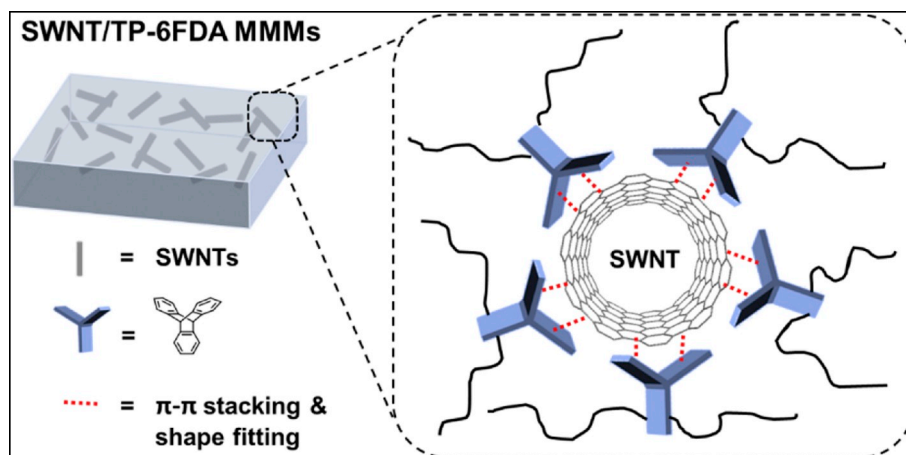**Fig. 2.** Structure of 6FDA-TP polyimide.

Fig. 1. Schematic illustration of π-π stacking and supramolecular shape-fitting interactions between triptycene units and SWNTs in mixed-matrix membranes.

membranes was as follows: 0.17 g 6FDA-TP polymer was dissolved in 2.5 ml DMF and filtered using a 0.45 μm syringe filter. Predetermined amount of AP-SWNTs was homogeneously dispersed in 1.5 ml DMF by sonication for 2 h at room temperature. Then, the polymer solution was transferred into AP-SWNTs suspensions in three rounds, with 15 min magnetic stirring and 30 min sonicating between each round, to obtain the casting solutions. The polymer concentration of the casting solutions was 4 w/v% and the blend ratios of filler to polymer were 2, 5, 10 and 15 wt% respectively. The casting solutions were poured onto a leveled glass plate and dried under IR lamp until formation of solid films. The films were immersed in methanol for 24 h for solvent exchange and further dried in vacuum oven at 160 °C overnight to ensure complete removal of residual solvent. Using the same casting method, 2 wt% P-SWNT/6FDA-TP and 2 wt% A-SWNT/6FDA-TP composite membranes were also prepared.

2.5. Characterization methods

The morphologies of carbon nanotubes and resulting composite films were examined using the field emission scanning electron microscopy (FESEM, FEI-MAGELLAN 400). Carbon nanotubes samples were prepared by adhering onto stainless steel stubs with carbon tapes. Film samples were prepared by breaking manually in liquid nitrogen. The samples were coated with a thin layer of gold before imaging.

The topography of carbon nanotubes was characterized using a Bruker Dimension Icon Atomic Force Microscope (AFM) for scanning probe microscopy in ScanAsyst/PeakForce Tapping mode, with silicon nitride ScanAsyst-air probes (Bruker). Over 100 nanotubes were measured using ImageJ software to obtain an average number of the dimension of carbon nanotubes.

The IR spectra of carbon nanotubes were taken with a Bruker Tensor 27 Fourier-Transformed Infrared spectroscopy with diffuse reflectance mode (DRIFT-FTIR). The samples were dried before being mixed with potassium bromide (KBr) powder to prepare a pellet for IR measurements. The spectrometer collected 128 scans in the range of 400–4000 cm^{-1} with a resolution of 4 cm^{-1}. For composite films, the IR spectra were taken in the same instrument with the attenuated total reflection (ATR) mode.

Raman spectra were taken using a Jasco NRS-5100 Micro-Raman Spectrometer in the range of 100–2000 cm^{-1} using an excitation wavelength of 532 nm. The laser power was 5 mW with a slit of 100 × 1000 μm.

The fluorescence spectra were measured using a Fluorolog-3 spectrofluorometer (Jobin Yvon Horiba). The samples were prepared by cutting the films into small pieces that just fit in the glass cuvette. An excitation wavelength of 285 nm with a 340 nm filter was applied for the measurement.

The thermal stability of the SWNTs and the composite membranes were investigated by using TGA Q500 (TA instruments), wherein fully dried thin films were heated at a rate of 10 °C min^{-1} from 50-800 °C under a nitrogen environment.

The glass transition temperatures of pristine polyimide membrane and composite membranes were investigated using a differential scanning calorimetry (DSC Q2000, TA Instruments). A heat/cool/reheat profile was used from 25 to 400 °C, with a heating rate of 10 °C min^{-1} and cooling rate of 20 °C min^{-1} under nitrogen atmosphere. The second heating profile was recorded to determine the glass transition temperature.

Wide-angle X-ray diffraction (WAXD) was employed to characterize polymer chain packing efficiency in the membranes. A Bruker D8 Advance DAVINCI diffractometer with Cu Kα radiation (wavelength λ = 1.54 Å) was used. The measurements were performed with 2θ ranging from 5° to 45°, a scan size of 0.02°/step and a scan speed of 5 s/step.

2.6. Pure gas permeation test

Pure gas permeabilities of H_2, CH_4, N_2, O_2, and CO_2 were tested following the order. A custom-built permeation system was used to perform the measurement based on constant-volume, variable-pressure method [32]. All samples were prepared as described previously and degassed overnight prior to measurement [28,33]. The gas permeation tests were conducted at 35 °C under predetermined feed pressures ranging from 3.0 to 16.6 atm. After reaching steady state, the rate of downstream pressure increase was recorded to calculate the permeability using the following equation:

$$P = \frac{V_d l}{p_{up} ATR} \left[\left(\frac{dp}{dt} \right)_{ss} - \left(\frac{dp}{dt} \right)_{leak} \right] \left(1 \times 10^{10} \right)$$

where P is the pure gas permeability in Barrer (1 Barrer = 1 × 10^{-10} cm^3(STP)·cm/cm^2·s·cmHg), V_d is the downstream reservoir volume (cm^3), l is the membrane thickness (cm), p_{up} is the upstream pressure (cmHg), A is the effective membrane area (cm^2), (dp/dt)$_{leak}$ is the leak rate of the system (cmHg/s) at 35 °C, T is the operating temperature (K), and R is the gas constant (0.278 cm^3·cmHg/cm^3(STP)·K). The ideal selectivity ($\alpha_{A/B}$) for two gases A and B was defined as the ratio of pure gas permeability of these two gases where A is the more permeable gas. The testing area of the samples was determined using a digital scanner (LiDE120, Canon) and ImageJ software. The thickness of the samples was measured using a digital micrometer.

The diffusion coefficient D (cm^2·s^{-1}) was determined using the lag-time method based on the following equation [32,34]:

$$D = \frac{l^2}{6\theta}$$

where l is the film thickness (cm) and θ is the lag time (s). The solubility coefficient S (cm^3(STP)/(cm^3·atm)) was calculated from pure-gas permeability (P) and diffusion coefficient (D) based on the solution-diffusion model:

$$P = S \times D$$

3. Results and discussion

3.1. Characterization of single-walled carbon nanotubes (SWNTs)

The topology of pristine AP-SWNTs and acid-treated A-SWNTs was investigated by SEM and AFM, particularly the length of SWNT bundles. As revealed in Fig. 3(a), in pristine AP-SWNT, lots of spherical impurities could be observed, which were the metallic catalyst residuals from the manufacturing process according to the manufacturer [35]. After purification by nitric acid solution, P-SWNT sample showed much less impurities as metallic catalysts were mostly oxidized and dissolved in acid solution. However, there was no significant change in aspect ratio (Fig. 3 (b) and Fig. S1) [36]. The strong acid-treated A-SWNT showed almost no spherical metallic catalysts, with a small amount of carbon impurities left on the sidewall of A-SWNTs as shown in SEM and AFM images of Fig. 3c-d [27,37,38].

The average length of pristine AP-SWNT bundles was in a range of 1–5 μm as provided by the manufacturer. The same average length was observed in the purified P-SWNTs according to SEM. The length distribution of A-SWNTs was determined via image analysis in a range of 0.1 μm–1.5 μm with an estimated average length of 0.4 μm. The much shorter length of A-SWNTs than that of AP-SWNTs indicated successful cutting of carbon nanotubes after strong acid treatment. The first step of nitric acid purification could not only remove metallic impurities, but also introduce vulnerable sites that allow oxidative cutting in strong acid treatment [39].

The integrity of SWNTs after cutting was verified by Raman spectra as shown in Fig. S2 in the Supporting Information. For all SWNTs, the
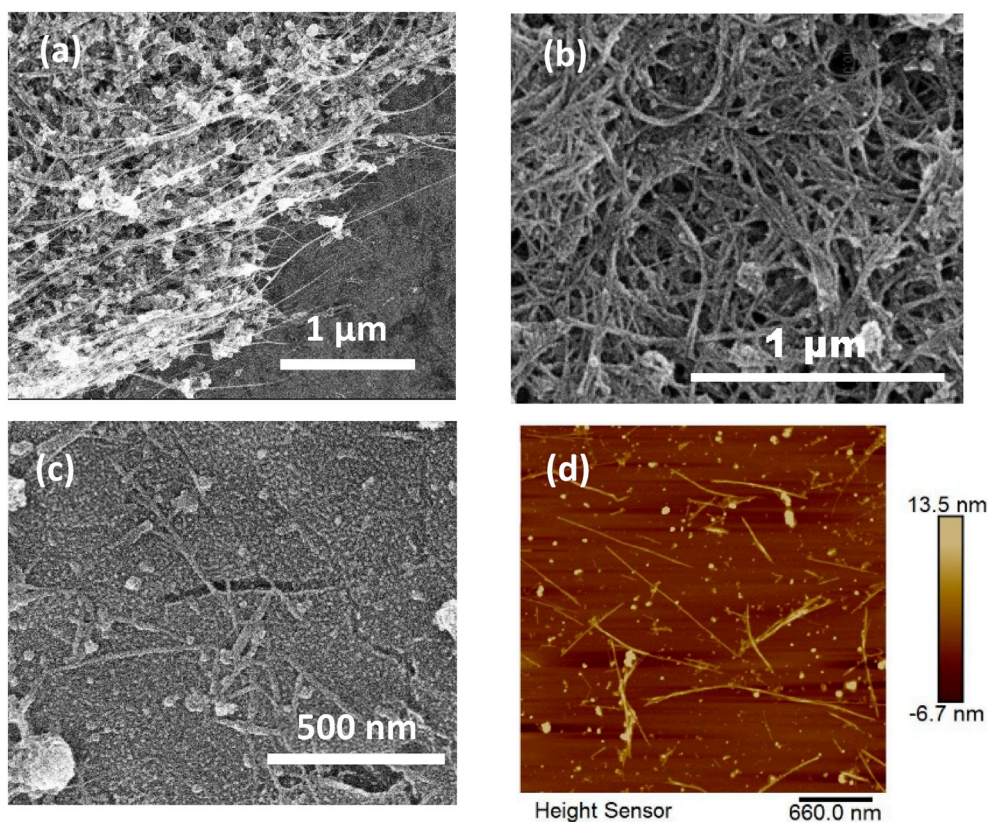
Fig. 3. SEM image of (a) AP-SWNT obtained from manufacturer, with long carbon nanotubes fibers and spherical metallic impurities, and (b) P-SWNT with removed metallic impurities. (c–d) SEM and AFM image of acid-treated A-SWNT respectively.

peaks at ~1580 cm^{-1} correspond to the G-bands of graphene sheets from carbon walls. The small peak at about 160 cm^{-1} is the characteristic peak of SWNT from the nanotube radial breathing modes (RBM) [40]. Also, the average diameter of individual carbon nanotubes was 1.4 nm according to the manufacturer, which was considered unchanged after surface modification as evidenced by the presence of the same RBM peaks. The disordered sp^2 carbon induced D-band appeared at ~1300 cm^{-1} in both P-SWNTs and A-SWNTs owing to the changed environment of carbon atoms upon acid treatment [41].

The purities of the carbon nanotubes were also examined by TGA analysis in air atmosphere. According to Fig. S3 in the Supporting Information, the residual weight of AP-SWNTs after burning was much higher than P-SWNTs and A-SWNTs, suggesting successful removal of metal impurities in P-SWNTs and A-SWNTs. All carbon nanotubes revealed a three-step weight loss behavior. The first step was the burning of amorphous carbon (around 350–400 °C). The second and the most noticeable weight loss was at around ~500–600 °C, which was due to thermal degradation of carbon nanotubes. The last peak at > 600 °C could be assigned to other stable carbonaceous materials from manufacture [36]. It is obvious that after the purification and acid treatment, the weight loss derivative curve of amorphous peak is much smaller and the SWNT degradation peak was broader with higher intensity, which was due to the exfoliation and degradation of amorphous carbons during acid treatment [42].

The surface functionality of SWNTs also changed after acid treatment. The FTIR spectra of AP-SWNT, P-SWNT and A-SWNT are depicted in Fig. S4 in the Supporting Information. The peaks at 1634 cm^{-1}, 2929 cm^{-1} and 2851 cm^{-1} represented the carbon skeleton and C–H bonds of alkyls, which were characteristic peaks of SWNTs. The broad peak at 3448 cm^{-1} and the small peak at 1028 cm^{-1} was due to hydroxyl groups from either the oxidized carbon nanotubes or the atmospheric moisture. The intensity of the peaks increased after acid treatment, which is a sign

of O–H bonds introduced to the surface of A-SWNT [42]. Furthermore, a small peak at around 1389 cm^{-1} is due to the presence of O–H bending of carboxylic acid groups. Also, a tiny peak at 1714 cm^{-1} appeared in correspondence to C=O stretching. The FTIR spectra evidence the formation of –OH and –COOH groups on the surface of acid treated SWNTs [24]. The properties of all three types of SWNTs are summarized in Table 1 and were used as fillers for preparation of MMMs as discussed later.

3.2. Characterization of AP-SWNT/6FDA-TP MMMs with varying filler content

The dispersion of fillers and the interfacial morphology between phases in MMMs are critical for desired gas separation performance. To explore the effect of π-π interaction between the carbon nanotubes and the benzene rings of tripytcene moieties of the polymer matrix on interfacial morphology, a series of composite membranes with systematically varied AP-SWNT content (2 wt%, 5 wt%, 10 wt%, and 15 wt%)

Table 1
Summary of filler properties, including carbonaceous purity, bundle length and surface functionality.

	AP-SWNT[a]	P-SWNT	A-SWNT
Carbonaceous purity	60–70%	>90%	>90%
Bundle length (μm)	1–5	1–5[b]	~0.1–1.5[c]
Surface functionality	none	-COOH (low content)	-COOH (high content)

[a] Reported by the manufacturer.
[b] The purification step simply removed the metallic impurities and changed surface functionality. No significant effect on length was observed.
[c] The average length was 0.4 μm according to AFM image analysis.

were prepared. In all cases, homogeneous, defect-free and ductile thin films were obtained indicating successful fabrication protocols (Fig. S5). The cross-sectional SEM images of pristine 6FDA-TP film and the composite membranes were obtained and the representative images are shown in Fig. 4. As can be seen, the pure 6FDA-TP polyimide film had a dense and smooth cross section. Alternatively, AP-SWNT membranes had much rougher cross-section morphology due to the good compatibility between carbon nanotubes and polymer matrix. During sample fracture in liquid nitrogen, the strong adhesive interactions between carbon nanotubes and polymer matrix created stress and consequently led to local plastic deformation, resulting in rough fracture surfaces [6, 43]. At the highest loading of 15 wt%, the carbon nanotubes were more entangled together due to high aspect ratio, high surface energy and high content [44]. Nevertheless, the nanofibers were still well dispersed across the polymer matrix without visible aggregation, suggesting that the high compatibility between nanotubes and polymer chain resulted in defect-free morphology of MMMs, as shown in Fig. S6. The strong affinity between the filler and matrix phases was likely realized through π-π interaction between graphene walls of nanotubes and benzene rings of triptycenes, as well as increased van der Waals force associated with the exquisite shape-fitting of carbon nanotubes into the clefts between benzene "blades" of triptycene units (Fig. 1).

Raman spectroscopy was applied to characterize single-walled carbon nanotubes in MMMs and to further confirm the favorable interaction between nanotubes and polymer matrix. According to Fig. 5(a), three peaks at around 1580 cm^{-1}, 1560 cm^{-1} and 160 cm^{-1} could be observed in all composite films, representing characteristic G$^+$, G$^-$ and RBM bands of single-walled carbon nanotubes. The RBM peak up-shifted comparing with pristine AP-SWNT, which was attributed to augmented charge transfer of π-electrons between carbon nanotubes and polymer matrix [31,45,46].

The fluorescence spectroscopy was demonstrated to further evidence the interaction between carbon nanotubes and the triptycene-based polyimide. The fluorescence spectra of 6FDA-TP polyimide membrane and AP-SWNT MMMs with a variety of loadings are shown in Fig. 5(b). An emission peak at 502 nm was observed for the pure polyimide film, which was due to the aromatic rings in the polyimide backbones [47].

However, significant quenching occurred after the incorporation of AP-SWNTs in all MMMs. This phenomenon indicated the electronic transfer from the triptycene moieties to carbon nanotubes, which was promoted by the strong π-π stacking interactions between graphene carbon walls and triptycene moieties in the polyimide [31,48].

It is well known that the improved filler-polymer interfacial interaction and corresponding polymer rigidification generally lead to increased glass transition temperature (T$_g$) [49,50]. The effect of AP-SWNT fillers to polymer chain packing was investigated by DSC. As indicated in Fig. 6(a), T$_g$ of the film with 2 wt% AP-SWNT was almost identical to that of pristine polymer, then it increased very slightly with increasing filler content. This indicates that the interfacial interaction in all MMMs only locally restricted polymer chain mobility. Moreover, it may imply that π-π stacking and supramolecular shape-induced nano-confinement between triptycene units and SWNTs are not only able to increase interfacial affinity but also largely retain the flexibility of polymer chains, which advantageously avoids significant surface rigidification and consequent reduction in diffusion as frequently observed in composite membranes [51,52]. Additionally, all AP-SWNT containing composite films showed well-maintained thermal stability, as revealed by TGA profiles shown in Fig. 6(b). This could be related to the high thermal stability of AP-SWNT and good filler-polymer affinity [53].

WAXD patterns of 6FDA-TP and AP-SWNT/6FDA-TP MMMs are illustrated in Fig. 7 to study the changes in inter-chain spacing of the polymers upon the addition of SWNTs. For the pristine triptycene-based polyimide membrane, it has three peaks at 2θ = 13.2°, 17.1° and 22.2°, representing *d*-spacing from amorphous polymer chain packing, tighter packing of chain segments without triptycene moieties, and π-π stacking, respectively [54]. For all the composite membranes, the appearance of two small sharp peaks at 27.4° and 44° are due to crystallinity of AP-SWNTs, which are in correspondence of (002) and (100) reflections [55,56]. The intensity of the first and second peaks (peak A and peak B) decreased with increasing AP-SWNT content, which might be due to the disruption of chain packing of the polyimide [24]. However, the relative intensity of the third peak C increased by incorporating 2 wt% and 5 wt% of AP-SWNT into polymer matrix. This indicates that the introduction of carbon nanotubes into triptycene-based polyimide promoted π-π
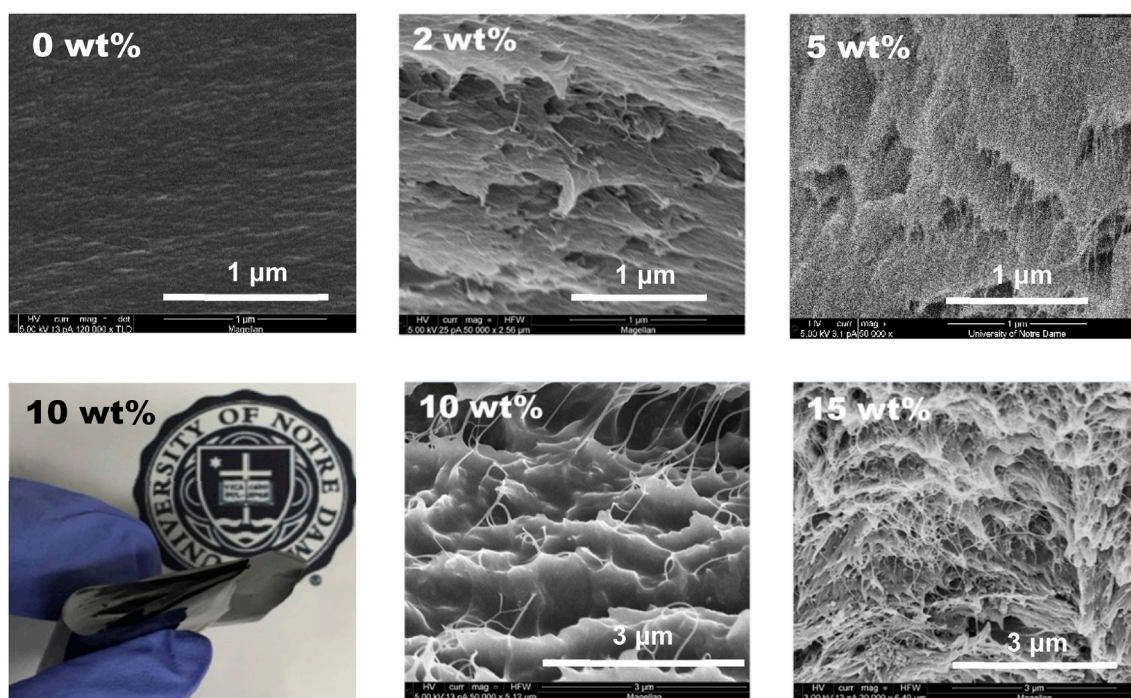

Fig. 4. Physical appearance of a 10 wt% AP-SWNT/6FDATP MMM (top left), and SEM cross-sectional images of pure 6FDA-TP polyimide membrane (bottom left) and AP-SWNT containing MMMs (middle and right) with 2 wt%, 5 wt%, 10 wt% and 15 wt% filler loadings.
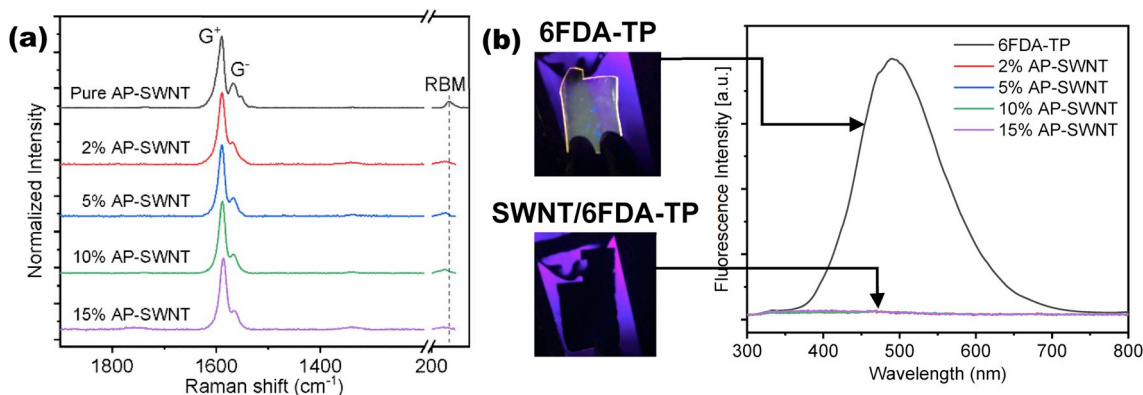
Fig. 5. (a) Raman spectra of pristine AP-SWNT and AP-SWNT/6FDA-TP MMMs. The shift of RBM peak of AP-SWNT in composite membranes due to augmented charge transfer between filler and polymer matrixn. (b) Fluorescence spectra of pure 6FDA-TP polyimide membrane and AP-SWNT MMMs. Inset pictures: (top) pure 6FDA-TP polyimide film was fluorescent under UV lamp and (bottom) quenched after addition of 2 wt% AP-SWNT.
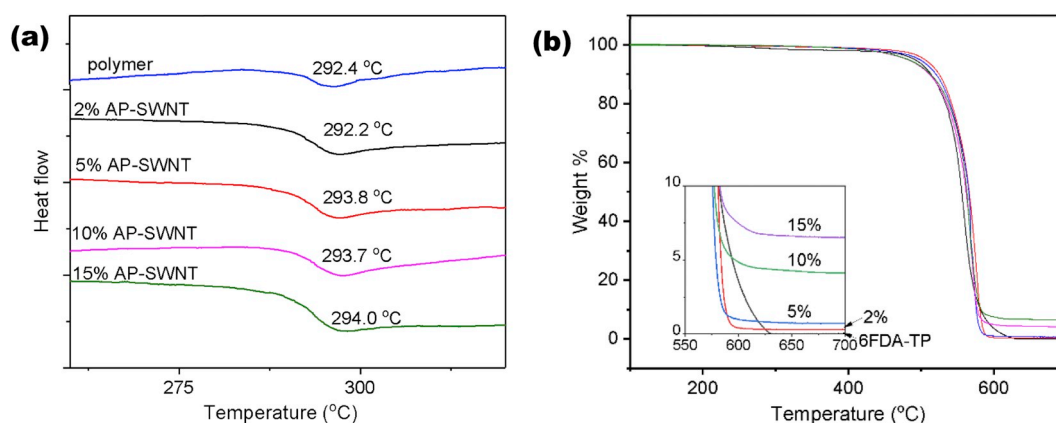

Fig. 6. (a) DSC and (b) TGA analysis of pure 6FDA-TP film and AP-SWNT/6FDA-TP MMMs at different filler loadings. The inset graph shows an enlarged view of the residual weights.
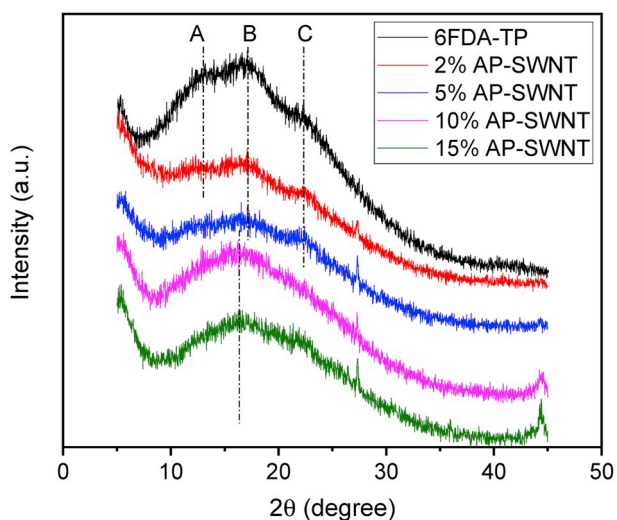

Fig. 7. WAXD patterns of 6FDA-TP polyimide film and AP-SWNT/6FDA-TP MMMs.

stacking interaction. As more fillers embedded in the polymer matrix, the polymer chain packing was further disrupted, leaving only one major peak at 16.4°. Compared to the pure polyimide membrane, the *d*-spacing of MMMs with high filler loadings increased slightly from 5.2

Å to 5.3 Å.

3.3. Effect of nanotube geometry and surface functionality on MMMs morphology

Membrane morphologies were examined as a function of the type of SWNTs to investigate the effect of nanotube geometry and surface functionality on interfacial properties in these composite membranes. Fig. 8 shows the cross-sectional SEM images of MMMs containing 2 wt% of AP-SWNT, P-SWNT and A-SWNT, respectively. The homogeneous dispersion of all types of fillers was confirmed without agglomeration and sedimentation across the film according to Fig. 8(a–c). Moreover, there is no evidence of interfacial defects between carbon nanotubes and polymer matrix, as shown in Fig. 8(a'-c'). Therefore, it could be concluded that the surface functionalization did not affect the strong interaction between carbon nanotubes and polymer matrix.

FTIR and DSC spectra of MMMs with different types of fillers are displayed in Fig. S7 in the Supporting Information. The FTIR spectra of the composite membranes are almost identical to the pure polyimide membranes, suggesting that the strong affinity between phases were physically bonded without chemical interaction. Similar to the MMMs composing non-modified AP-SWNTs, the T_g of composite membranes containing 2 wt% P-SWNT or 2 wt% A-SWNT almost unchanged compared to the pristine polyimide membrane according to Fig. S7(b). The presence of single-walled carbon nanotubes was confirmed by Raman spectra as depicted in Fig. S8 in the Supporting Information. Thermal stability of the membranes was characterized using TGA in air
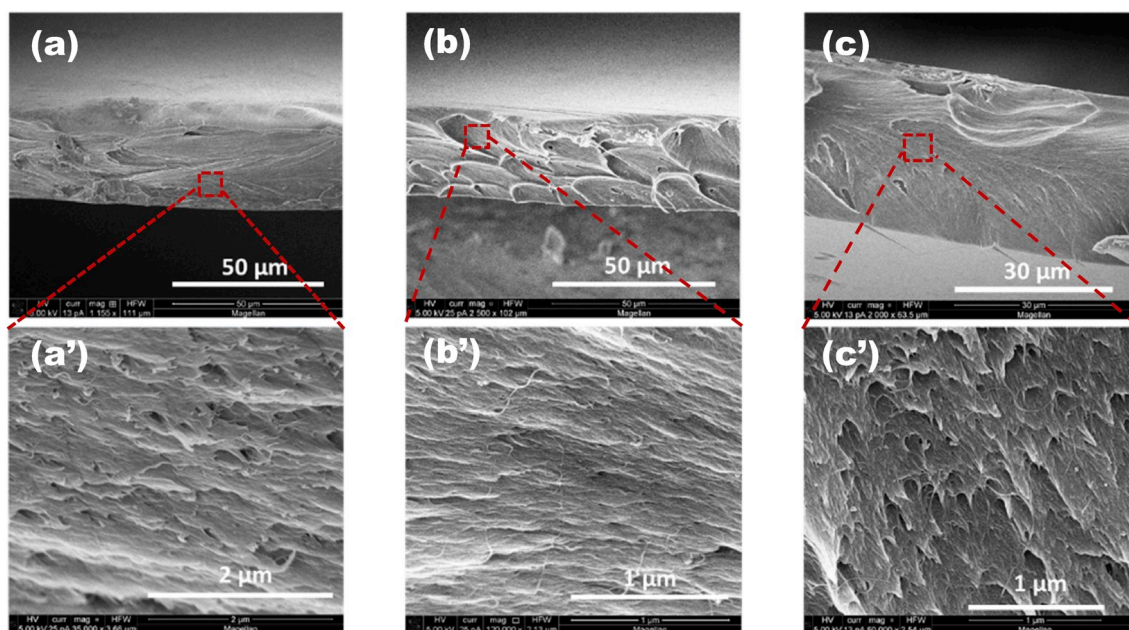
Fig. 8. Cross-sectional SEM images of MMMs with different type of fillers at 2 wt% filler content: (a) and (a') AP-SWNT; (b) and (b') P-SWNT; (c) and (c') 2 wt% A-SWNT.

atmosphere, as shown in Fig. S9. WAXD studies were also performed on the MMMs containing 2 wt% P-SWNT and A-SWNT aged for 27 months, shown in Fig. S10. There is no peak shift upon the incorporation of either non-functionalized or functionalized carbon nanotubes, indicating no noticeable change of *d*-spacing in the composite membranes. Similar to the AP-SWNT containing MMMs, the P-SWNT and A-SWNT containing MMMs also show high intensity of peak C, which is attributed to the π-π stacking between carbon nanotubes and aromatic rings in polymer backbone. The intensity change in peak A and B was attributed to the redistribution in fractional free volumes by aging, which has been discussed in our previous work [54].

3.4. Gas transport properties of MMMs

3.4.1. Effect of filler content

Pure gas permeabilities of H_2, CH_4, N_2, O_2 and CO_2 of pure 6FDA-TP film and AP-SWNT/6FDA-TP MMMs with various SWNT content were measured and ideal selectivities were calculated. The permeability and selectivity as a function of filler content are shown in Fig. 9 as well as summarized in Table S1. It can be observed that with 2 wt% of AP-SWNT incorporated into the polyimide, the permeabilities increased significantly for all gases. For example, the permeability of CO_2 increased by 300% from 20 Barrer of pure polymer to 81 Barrer after adding 2 wt% of

AP-SWNT. However, at 5 wt% AP-SWNT content, the permeabilities of all gases decreased as depicted in Fig. 9(a), although still higher than pure polyimide film. When combining more AP-SWNTs into the polymer, the permeabilities of most gases showed increasing pattern except for H_2. The enhancement in permeabilities could be ascribed to the rapid diffusion of gas molecules inside the nanotubes due to the super smooth inner wall, and the disrupted polymer chain packing by embedded carbon nanotubes that increased the fractional free volume [44,57]. Since large gas molecules are more sensitive to free volume change, the increase in permeability of large molecule gases (e.g., CH_4, N_2) are more significant than H_2. Some researchers also reported decreased permeabilities in carbon nanotubes containing mixed matrix membranes at high filler loadings [24,58]. For example, Sun et al. studied the gas transport performance of pristine and functionalized multi-walled carbon nanotubes in DMMDA-BTDA polyimide and found that permeabilities of CO_2 and CH_4 exhibited a decreasing trend with loading above 4 wt% due to agglomeration and cluster of nanofibers [24]. However, the SEM images showed homogeneous dispersion of carbon nanotubes without noticeable aggregation in this study. Thus, the slightly lower H_2 permeability at the highest AP-SWNT loading might be due to more non-permeable carbon walls that act as transport barriers to block the fast diffusion of H_2 molecules.

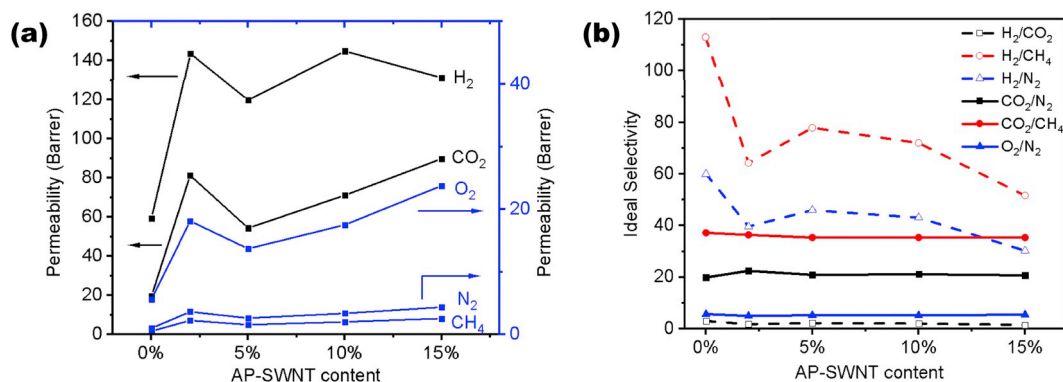Fig. 9(b) shows selectivities of different gas pairs versus filler

Fig. 9. Effects of AP-SWNT content on (a) pure gas permeability, and (b) ideal selectivity.

content. H_2 separation performance was largely affected by the addition of AP-SWNTs, and the selectivities decreased with increasing AP-SWNT content. Again, this was due to larger improvement in permeabilities of large molecule gases than that of H_2. However, for other gas pairs including CO_2/N_2, CO_2/CH_4 and O_2/N_2, the selectivities were relatively comparable to the pure polyimide membrane, indicating good interfacial morphology in all MMMs that benefits from the strong interfacial interaction between carbon nanotubes and triptycene moieties in polymer backbone.

Diffusivity and solubility coefficients for CH_4, N_2 and CO_2 were obtained from lag-time method to probe the transport mechanism in the MMMs and the data are summarized in Table S2 and Fig. S11 in the Supporting Information. The trend of diffusivity coefficients as a function of AP-SWNT content is similar to the permeabilities for corresponding gases, and the solubilities are relatively stable at different loadings. Hence, the variation in permeability is mainly controlled by kinetic diffusion in these composite membranes.

The permeability/selectivity trade-off plot for CO_2/CH_4 with Robeson's upper bound is illustrated in Fig. 10. Some reported data for carbon nanotubes containing MMMs are also shown for comparison. As a general trend, incorporating SWNTs in triptycene-based polyimides significantly improves the permeability-selectivity combinations by pushing the overall separation performance laterally approaching the upper bound. It appears that the membrane with 2 wt% of AP-SWNT has the most desirable interfacial morphology with balanced filler-polymer interactions. Compared to other MMMs composing CNTs and non-triptycene-containing glassy polymers, our membrane showed greatly enhanced permeability at much lower filler content, without sacrificing selectivity. Based on this result, a fixed 2 wt% filler loading was chosen for further studies to investigate the effects of SWNTs' dimension (e.g., bundle length) and surface functionality on gas transport properties as discussed in following section.

3.4.2. Effect of carbon nanotube length and surface functionality on gas transport properties

As discussed previously, the incorporation of carbon nanotubes could significantly improve the gas transport properties due to the rapid gas diffusion through the barrier-free inner channels. On the other hand, in MMMs with high SWNT content, the impermeable carbon wall of nanotubes and non-carbonaceous impurities seem to hinder gas diffusion that decrease the gas permeability possibly due to the formation of

interconnected network via entanglement of long nanotube bundles. To examine how nanotube bundle length may affect the gas transport, purified and shortened carbon nanotubes, i.e., P-SWNTs and A-SWNTs (Table 1), were prepared from AP-SWNTs via strong acid treatment and used to prepare MMMs. It is expected that with smaller aspect ratio and higher purity, the entanglement of long nanotube bundles could be reduced, and more open ends would appear to allow gas molecules entering and passing through. Additionally, the cutting procedure using strong acid can introduce carboxylic acid functional groups on the surface of SWNTs, which may possibly assist selective separation of polar gases.

MMMs with 2 wt% of different type of fillers (AP-SWNT, P-SWNT and A-SWNT) were prepared and the pure gas permeabilities were tested following the same procedure. The permeation data are summarized in Table 2. Regardless of different physical properties of carbon nanotubes, all composite membranes showed significantly higher permeabilities than the pure 6FDA-TP membrane for all gases, indicating that SWNTs effectively introduce barrier-free gas transport pathways in the MMMs. Among the three MMMs, with the same weight loading, purified and shorter nanotubes led to slightly reduced permeabilities likely due to fewer interface defects induced by the metallic impurities. However, marked increases in ideal selectivities for all gas pairs are observed in the MMMs containing purified and shorter nanotubes compared to AP-SWNT containing membrane. Moreover, the membrane with 2 wt% A-SWNT showed overall better separation performance than the pure polyimide film in terms of both permeability and selectivities.

To elucidate the fundamental transport properties, the diffusivity and solubility coefficients and corresponding diffusivity and solubility selectivities were calculated and are shown in Table S3 in the Supporting Information. With 2 wt% A-SWNTs, the diffusivity coefficients enhanced for all gases, implying that gas molecules had higher chance to enter the shortened carbon nanotubes for fast diffusion than in the membranes containing AP-SWNTs and P-SWNTs. As shown in Table 1, the acid treated A-SWNT had a shortened average length of 0.4 μm, which was much larger than the kinetic diameter of gas molecules. It is logical to expect that by further decreasing the length of SWNTs, enhanced gas diffusion could originate from much less entanglement of SWNTs, more open pores as barrier-free gas transport channels, and potentially better SWNT alignment at the same filler loading. In this regard, systematic studies on the lengths of SWNTs and optimized filler contents are needed for future study, which may open a new dimension in preparing CNT-based MMMs. Additionally, the improved carbonaceous purity also played a role in enhancing the interfacial morphology and gas transport properties. Another important factor affecting the separation
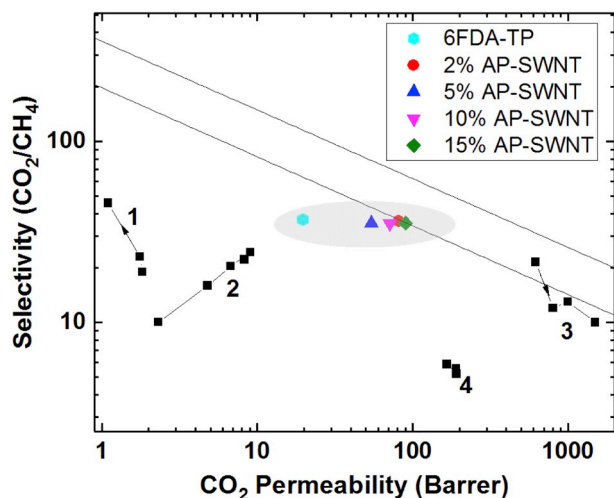

Fig. 10. CO_2/CH_4 permeability/selectivity upper bound plot for AP-SWNT/6FDA-TP MMMs. Other comparative data are: 1) 0, 1, 6 wt% MWCNT/PI MMMs [51]; 2) 0, 1, 2, 3, 4 wt% MWCNT/PI MMMs [24]; 3) 0, 5, 10, 15 wt% CNT-COOH/6FDA-durene MMMs [59]; and 4) 0, 2, 10 wt% SWCNT/poly(imide siloxane) MMMs [60].

Table 2

Pure gas permeation data of 6FDA-TP membrane and the MMMs with 2 wt% of AP-SWNT, P-SWNT and A-SWNT for comparison.

	Permeability (Barrer)				
	H_2	CH_4	N_2	O_2	CO_2
6FDA-TP[a]	59	0.5	1.0	5.6	20
2% AP-SWNT	144 ± 2	2.2 ± 0.1	3.6 ± 0.1	18 ± 0.2	81 ± 1
2% P-SWNT	140 ± 3	1.9 ± 0.1	3.2 ± 0.1	18 ± 0.4	74 ± 2
2% A-SWNT	122 ± 3	1.4 ± 0.1	2.7 ± 0.1	17 ± 0.4	63 ± 1

	Ideal Selectivity					
	H_2/CH_4	H_2/N_2	H_2/CO_2	CO_2/N_2	CO_2/CH_4	O_2/N_2
6FDA-TP[a]	113	60	3.0	20	37	5.6
2% AP-SWNT	64 ± 1	40 ± 1	1.8 ± 0.1	22 ± 0.2	36 ± 1	5.0 ± 0.1
2% P-SWNT	75 ± 3	44 ± 1	1.9 ± 0.1	23 ± 0.8	39 ± 1	5.7 ± 0.2
2% A-SWNT	88 ± 3	45 ± 2	1.9 ± 0.1	23 ± 0.7	46 ± 2	6.1 ± 0.2

[a] Pure 6FDA-TP permeability and selectivity are adapted from Ref. [28].

performance seems to be the surface functionality. It has been reported that –COOH groups on the surface of carbon nanotubes can increase the affinity of polar gases such as CO_2 [24]. According to Table S3, the improvement in overall selectivity mainly came from the increased solubility selectivities, which could be ascribed to the surface functionality change in P-SWNTs and A-SWNTs.

The overall separation performance for MMMs is compared with the Robeson's upper bounds in Fig. 11. In general, using the acid-treated, shortened A-SWNTs as filler produced composite membrane with the best overall performance. With a notable enhancement in selectivity and minor loss in permeability, the separation performance for CO_2/CH_4, O_2/N_2 and H_2/CH_4 gas pairs all shifted upward vertically compared to 2 wt% AP-SWNT MMM and surpassed the 1991 Robeson's upper bound. The improvement was due to the synergetic effects of a smaller aspect ratio of the carbon nanotubes, higher carbonaceous purity and –COOH surface functionality, which led to strong interactions between carbon nanotubes and triptycene-based polyimide allowing for the formation of ideal interfacial morphology and consequently enhanced gas separation performance of the composite membranes.

4. Conclusion

Mixed matrix membranes were successfully prepared by embedding different types of SWNTs (as-purchased, purified and acid-treated) into triptycene-based polyimide matrix. The purification step removed metallic catalyst residuals, and the strong acid treatment introduced carboxylic acid functionality to the surface of carbon nanotubes, as well as shortening the nanotubes. AP-SWNTs were well dispersed in polymer matrix without visible interfacial voids and agglomeration even at a high loading of 15 wt% according to SEM, highlighting the excellent

compatibility between fillers and polymer matrix. The pure gas permeabilities of the MMMs showed nonlinear trend with increasing filler loadings, which was due to the competition between enhanced gas transport through inner of carbon nanotubes and hampered gas diffusion by the carbon walls. Significant improvement in selectivities was observed in the MMMS containing purified and shortened SWNTs. Remarkably, the 2 wt% A-SWNT/6FDA-TP membrane exhibited both high permeabilities and selectivities compared to the pure 6FDA-TP polyimide membrane, locating the performance above the 1991 Robeson's upper bound for CO_2/CH_4, O_2/N_2 and H_2/CH_4. The remarkably improved performance could be attributed to: the carbon nanotubes with smaller aspect ratio that had more open ends for gas molecules to pass through; the functionalized surface of carbon nanotubes that improved the solubility selectivity; the higher purity of the modified carbon nanotubes as fillers.

Declaration of competing interest

The authors declare that they have no known competing financial interests or personal relationships that could have appeared to influence the work reported in this paper.

CRediT authorship contribution statement

Qinnan Zhang: Investigation, Writing - original draft. **Si Li:** Investigation. **Ceming Wang:** Investigation, Resources. **Hsueh-Chia Chang:** Resources. **Ruilan Guo:** Conceptualization, Methodology, Supervision, Writing - review & editing.
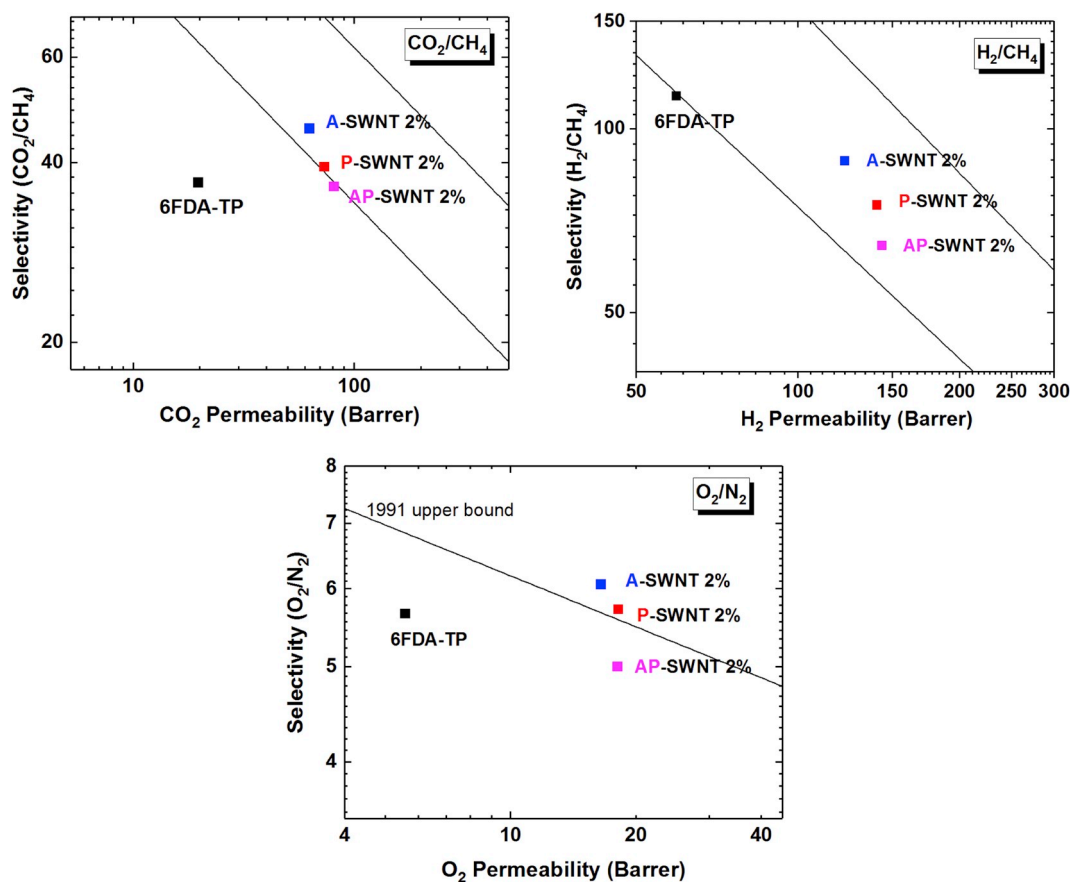
Fig. 11. Permeability/selectivity trade-off plots for CO_2/CH_4, H_2/CH_4 and O_2/N_2 gas pairs comparing the separation performance of pure 6FDA-TP membrane and MMMs containing 2 wt% AP-SWNT, P-SWNT and A-SWNT/6FDA-TP as labeled.

Appendix A. Supplementary data

Supplementary data to this article can be found online at https://doi.org/10.1016/j.memsci.2019.117794.

References

[1] W.J. Koros, G.K. Fleming, Membrane-based gas separation, J. Membr. Sci. 83 (1993) 1–80.

[2] S. Roussanaly, R. Anantharaman, K. Lindqvist, H. Zhai, E. Rubin, Membrane properties required for post-combustion CO_2 capture at coal-fired power plants, J. Membr. Sci. 511 (2016) 250–264.

[3] T.C. Merkel, H. Lin, X. Wei, R. Baker, Power plant post-combustion carbon dioxide capture: an opportunity for membranes, J. Membr. Sci. 359 (2010) 126–139.

[4] L.M. Robeson, The upper bound revisited, J. Membr. Sci. 320 (2008) 390–400.

[5] L.M. Robeson, Correlation of separation factor versus permeability for polymeric membranes, J. Membr. Sci. 62 (1991) 165–185.

[6] G. Dong, H. Li, V. Chen, Challenges and opportunities for mixed-matrix membranes for gas separation, J. Mater. Chem. A. 1 (2013) 4610–4630.

[7] H. Bux, F. Liang, Y. Li, J. Cravillon, M. Wiebcke, Zeolitic imidazolate framework membrane with molecular sieving properties by microwave-assisted solvothermal synthesis, J. Am. Chem. Soc. 131 (2009) 16000–16001.

[8] M. Vinoba, M. Bhagiyalakshmi, Y. Alqaheem, A.A. Alomair, A. Pérez, M.S. Rana, Recent progress of fillers in mixed matrix membranes for CO_2 separation: a review, Separ. Purif. Technol. 188 (2017) 431–450.

[9] M. Benzaqui, R. Semino, N. Menguy, F. Carn, T. Kundu, J. Guigner, N.B. Mckeown, K.J. Msayib, M. Carta, R. Malpass-evans, L. Guillouzer, G. Clet, N.A. Ramsahye, C. Serre, G. Maurin, N. Steunou, Toward an understanding of the microstructure and interfacial properties of PIMs/ZIF-8 mixed matrix membranes, ACS Appl. Mater. Interfaces 8 (2016) 27311–27321.

[10] J. Dechnik, J. Gascon, C. Doonan, C. Janiak, C.J. Sumby, New directions for mixed-matrix membranes, Angew. Chem. Int. Ed. 56 (2017) 9292–9310.

[11] T.T. Moore, W.J. Koros, Non-ideal effects in organic-inorganic materials for gas separation membranes, J. Mol. Struct. 739 (2005) 87–98.

[12] M. Rezakazemi, A. Ebadi Amooghin, M.M. Montazer-Rahmati, A.F. Ismail, T. Matsuura, State-of-the-art membrane based CO_2 separation using mixed matrix membranes (MMMs): an overview on current status and future directions, Prog. Polym. Sci. 39 (2014) 817–861.

[13] T.S. Chung, L.Y. Jiang, Y. Li, S. Kulprathipanja, Mixed matrix membranes (MMMs) comprising organic polymers with dispersed inorganic fillers for gas separation, Prog. Polym. Sci. 32 (2007) 483–507.

[14] N. Tien-Binh, H. Vinh-Thang, X.Y. Chen, D. Rodrigue, S. Kaliaguine, Polymer functionalization to enhance interface quality of mixed matrix membranes for high CO_2/CH_4 gas separation, J. Mater. Chem. A. 3 (2015) 15202–15213.

[15] R. Mahajan, W.J. Koros, Mixed matrix membrane materials with glassy polymers. Part 2, Polym. Eng. Sci. 42 (2002) 1432–1441.

[16] M.a. Aroon, a.F. Ismail, T. Matsuura, M.M. Montazer-Rahmati, Performance studies of mixed matrix membranes for gas separation: a review, Separ. Purif. Technol. 75 (2010) 229–242.

[17] T. Fukumaru, T. Fujigaya, N. Nakashima, Mechanical reinforcement of polybenzoxazole by carbon nanotubes through noncovalent functionalization, Macromolecules 46 (2013) 4034–4040.

[18] N.G. Sahoo, S. Rana, J. Whan, L. Li, S. Hwa, Polymer nanocomposites based on functionalized carbon nanotubes, Prog. Polym. Sci. 35 (2010) 837–867.

[19] A.I. Skoulidas, D.M. Ackerman, J.K. Johnson, D.S. Sholl, Rapid transport of gases in carbon nanotubes, Phys. Rev. Lett. 89 (2002) 185901.

[20] A.F. Ismail, P.S. Goh, S.M. Sanip, M. Aziz, Transport and separation properties of carbon nanotube-mixed matrix membrane, Separ. Purif. Technol. 70 (2009) 12–26.

[21] H. Chen, D.S. Sholl, Predictions of selectivity and flux for CH_4/H_2 separations using single walled carbon nanotubes as membranes, J. Membr. Sci. 269 (2006) 152–160.

[22] A.I. Skoulidas, D.S. Sholl, J.K. Johnson, Adsorption and diffusion of carbon dioxide and nitrogen through single-walled carbon nanotube membranes, J. Chem. Phys. 124 (2006).

[23] M.M. Khan, V. Filiz, G. Bengtson, S. Shishatskiy, M.M. Rahman, J. Lillepaerg, V. Abetz, Enhanced gas permeability by fabricating mixed matrix membranes of functionalized multiwalled carbon nanotubes and polymers of intrinsic microporosity (PIM), J. Membr. Sci. 436 (2013) 109–120.

[24] H. Sun, T. Wang, Y. Xu, W. Gao, P. Li, Q.J. Niu, Fabrication of polyimide and functionalized multi-walled carbon nanotubes mixed matrix membranes by in-situ polymerization for CO_2 separation, Separ. Purif. Technol. 177 (2017) 327–336.

[25] S.A. Habibiannejad, A. Aroujalian, A. Raisi, Pebax-1657 mixed matrix membrane containing surface modified multi-walled carbon nanotubes for gas separation, RSC Adv. 6 (2016) 79563–79577.

[26] C.A. Furtado, U.J. Kim, H.R. Gutierrez, L. Pan, E.C. Dickey, P.C. Eklund, Debundling and dissolution of single-walled carbon nanotubes in amide solvents, J. Am. Chem. Soc. 126 (2004) 6095–6105.

[27] W. Zhou, S. Sasaki, A. Kawasaki, Effective control of nanodefects in multiwalled carbon nanotubes by acid treatment, Carbon N. Y. 78 (2014) 121–129.

[28] J.R. Wiegand, Z.P. Smith, Q. Liu, C.T. Patterson, B.D. Freeman, R. Guo, Synthesis and characterization of triptycene-based polyimides with tunable high fractional free volume for gas separation membranes, J. Mater. Chem. A. 2 (2014) 13309–13320.

[29] J.R. Weidman, R. Guo, The use of iptycenes in rational macromolecular design for gas separation membrane applications, Ind. Eng. Chem. Res. 56 (2017) 4220–4236.

[30] T.M. Swager, Iptycenes in the design of high performance polymers, Acc. Chem. Res. 41 (2008) 1181–1189.

[31] S.Z. Zu, X.X. Sun, D. Zhou, B.H. Han, Supramolecular modification of single-walled carbon nanotubes with a water-soluble triptycene derivative, Carbon N. Y. 49 (2011) 5339–5347.

[32] H. Lin, B.D. Freeman, Permeation and diffusion, in: H. Czichos, T. Saito, L. Smith (Eds.), Springer Handb. Mater. Meas. Methods, Springer Berlin Heidelberg., Berlin, Heidelberg, 2006, pp. 371–387.

[33] Q. Zhang, S. Luo, J.R. Weidman, R. Guo, Preparation and gas separation performance of mixed-matrix membranes based on triptycene-containing polyimide and zeolite imidazole framework (ZIF-90), Polymer 131 (2017) 209–216.

[34] D.F. Sanders, Z.P. Smith, R. Guo, L.M. Robeson, J.E. McGrath, D.R. Paul, B.D. Freeman, Energy-efficient polymeric gas separation membranes for a sustainable future: a review, Polymer 54 (2013) 4729–4761.

[35] Carbon Solutions, Inc., 2019. (Accessed 25 October 2019). https://Www.Carbonsolution.Com/Faq.

[36] H. Hu, B. Zhao, M. Itkis, R. Haddon, Nitric acid purification of single-walled carbon nanotubes, J. Phys. Chem. B (2003) 13838–13842.

[37] M.W. Marshall, S. Popa-Nita, J.G. Shapter, Measurement of functionalised carbon nanotube carboxylic acid groups using a simple chemical process, Carbon N. Y. 44 (2006) 1137–1141.

[38] V.T. Le, C.L. Ngo, Q.T. Le, T.T. Ngo, D.N. Nguyen, M.T. Vu, Surface modification and functionalization of carbon nanotube with some organic compounds, Adv. Nat. Sci. Nanosci. Nanotechnol. 4 (2013), 035017.

[39] K.J. Ziegler, Z. Gu, H. Peng, E.L. Flor, R.H. Hauge, R.E. Smalley, Controlled oxidative cutting of single-walled carbon nanotubes, J. Am. Chem. Soc. 127 (2005) 1541–1547.

[40] A. Jorio, R. Saito, J.H. Hafner, C.M. Lieber, M. Hunter, T. McClure, G. Dresselhaus, M.S. Dresselhaus, Structural (n,m) determination of isolated single-wall carbon nanotubes by resonant Raman scattering, Phys. Rev. Lett. 86 (2001) 1118–1121.

[41] U.J. Kim, C.A. Furtado, X. Liu, G. Chen, P.C. Eklund, Raman and IR spectroscopy of chemically processed single-walled carbon nanotubes, J. Am. Chem. Soc. 127 (2005) 15437–15445.

[42] J. Zhang, H. Zou, Q. Qing, Y. Yang, Q. Li, Z. Liu, X. Guo, Z. Du, Effect of chemical oxidation on the structure of single-walled carbon nanotubes, J. Phys. Chem. B 107 (2003) 3712–3718.

[43] Y. Zhang, I.H. Musselman, J.P. Ferraris, K.J. Balkus, Gas permeability properties of Matrimid membranes containing the metal-organic framework Cu-BPY-HFS, J. Membr. Sci. 313 (2008) 170–181.

[44] Q. Xue, X. Pan, X. Li, J. Zhang, Q. Guo, Effective enhancement of gas separation performance in mixed matrix membranes using core/shell structured multi-walled carbon nanotube/graphene oxide nanoribbons, Nanotechnology 28 (2017), 065702.

[45] A. Chou, T. Böcking, R. Liu, N.K. Singh, G. Moran, J.J. Gooding, Effect of dialysis on the electrochemical properties of acid-oxidized single-walled carbon nanotubes, J. Phys. Chem. C 112 (2008) 14131–14138.

[46] M.S. Dresselhaus, G. Dresselhaus, R. Saito, A. Jorio, Raman spectroscopy of carbon nanotubes, Phys. Rep. 409 (2005) 47–99.

[47] H. Li, Q. Chen, B.-H. Han, Sugar-functionalized triptycenes used for dispersion of single-walled carbon nanotubes in aqueous solution by supramolecular interaction, New J. Chem. 40 (2016) 3300–3307.

[48] Y. Tomonari, H. Murakami, N. Nakashima, Solubilization of single-walled carbon nanotubes by using polycyclic aromatic ammonium amphiphiles in water - strategy for the design of high-performance solubilizers, Chem. Eur J. 12 (2006) 4027–4034.

[49] M.W. Anjum, F. Vermoortele, A.L. Khan, B. Bueken, D.E. De Vos, I.F.J. Vankelecom, Modulated UiO-66-based mixed-matrix membranes for CO_2 separation, ACS Appl. Mater. Interfaces 7 (2015) 25193–25201.

[50] S. Shahid, K. Nijmeijer, S. Nehache, I. Vankelecom, A. Deratani, D. Quemener, MOF-mixed matrix membranes: precise dispersion of MOF particles with better compatibility via a particle fusion approach for enhanced gas separation properties, J. Membr. Sci. 492 (2015) 21–31.

[51] M.a. Aroon, a.F. Ismail, M.M. Montazer-Rahmati, T. Matsuura, Effect of raw multi-wall carbon nanotubes on morphology and separation properties of polyimide membranes, Separ. Sci. Technol. 45 (2010) 2287–2297.

[52] P. Hammershøj, P.H.H. Bomans, R. Lakshminarayanan, J. Fock, S.H. Jensen, T.S. Jespersen, T. Brock-Nannestad, T. Hassenkam, J. Nygård, N.A.J.M. Sommerdijk, K. Kilså, T. Bjørnholm, J.B. Christensen, A triptycene-based approach to solubilising carbon nanotubes and C60, Chem. Eur J. 18 (2012) 8716–8723.

[53] T.H. Weng, H.H. Tseng, M.Y. Wey, Preparation and characterization of multi-walled carbon nanotube/PBNPI nanocomposite membrane for H_2/CH_4 separation, Int. J. Hydrogen Energy 34 (2009) 8707–8715.

[54] J.R. Weidman, S. Luo, C.M. Doherty, A.J. Hill, P. Gao, R. Guo, Analysis of governing factors controlling gas transport through fresh and aged triptycene-based polyimide films, J. Membr. Sci. 522 (2017) 12–22.

[55] a G. Rinzler, J. Liu, H. Dai, P. Nikolaev, C.B. Huffman, F.J. Rodríguez-Macías, P.J. Boul, a H. Lu, D. Heymann, D.T. Colbert, R.S. Lee, J.E. Fischer, a M. Rao, P.C. Eklund, R.E. Smalley, Large-scale purification of single-wall carbon nanotubes: process, product, and characterization, Appl. Phys. Mater. Sci. Process 67 (1998) 29–37.

[56] D.N. Futaba, K. Hata, T. Yamada, T. Hiraoka, Y. Hayamizu, Y. Kakudate, O. Tanaike, H. Hatori, M. Yumura, S. Iijima, Shape-engineerable and highly densely packed single-walled carbon nanotubes and their application as super-capacitor electrodes, Nat. Mater. 5 (2006) 987–994.

[57] J.K. Holt, H.G. Park, Y. Wang, M. Stadermann, A.B. Artyukhin, C.P. Grigoropoulos, A. Noy, O. Bakajin, Fast mass transport through sub-2-nanometer carbon nanotubes, Science 312 (2006) 1034–1037.

[58] B. Yu, H. Cong, Z. Li, J. Tang, X.S. Zhao, Pebax-1657 nanocomposite membranes incorporated with nanoparticles/colloids/carbon nanotubes for CO_2/N_2 and CO_2/H_2 separation, J. Appl. Polym. Sci. 130 (2013) 2867–2876.

[59] R. Lin, L. Ge, S. Liu, V. Rudolph, Z. Zhu, Mixed-matrix membranes with metal-organic framework-decorated CNT fillers for efficient CO_2 separation, ACS Appl. Mater. Interfaces 7 (2015) 14750–14757.

[60] S. Kim, T.W. Pechar, E. Marand, Poly(imide siloxane) and carbon nanotube mixed matrix membranes for gas separation, Desalination 192 (2006) 330–339.